


Bilayer Implants: Electromechanical Assessment of Regenerated Articular Cartilage in a Sheep Model

Cartilage
2016, Vol. 7(4) 346–360
© The Author(s) 2016
Reprints and permissions:
sagepub.com/journalsPermissions.nav
DOI: 10.1177/1947603515623992
cart.sagepub.com


Jan C. Schagemann^{1,2}, Nicola Rudert¹, Michelle E. Taylor², Sotcheadt Sim^{3,4},
Eric Quenneville⁴, Martin Garon⁴, Mathias Klinger⁵, Michael D. Buschmann³,
and Hagen Mittelstaedt¹

Abstract

Objective. To compare the regenerative capacity of 2 distinct bilayer implants for the restoration of osteochondral defects in a preliminary sheep model. **Methods.** Critical sized osteochondral defects were treated with a novel biomimetic poly- ϵ -caprolactone (PCL) implant (Treatment No. 2; $n = 6$) or a combination of Chondro-Gide and Orthoss (Treatment No. 1; $n = 6$). At 19 months postoperation, repair tissue ($n = 5$ each) was analyzed for histology and biochemistry. Electromechanical mappings (Arthro-BST) were performed *ex vivo*. **Results.** Histological scores, electromechanical quantitative parameter values, dsDNA and sGAG contents measured at the repair sites were statistically lower than those obtained from the contralateral surfaces. Electromechanical mappings and higher dsDNA and sGAG/weight levels indicated better regeneration for Treatment No. 1. However, these differences were not significant. For both treatments, Arthro-BST revealed early signs of degeneration of the cartilage surrounding the repair site. The International Cartilage Repair Society II histological scores of the repair tissue were significantly higher for Treatment No. 1 (10.3 ± 0.38 SE) compared to Treatment No. 2 (8.7 ± 0.45 SE). The parameters cell morphology and vascularization scored highest whereas tidemark formation scored the lowest. **Conclusion.** There was cell infiltration and regeneration of bone and cartilage. However, repair was incomplete and fibrocartilaginous. There were no significant differences in the quality of regeneration between the treatments except in some histological scoring categories. The results from Arthro-BST measurements were comparable to traditional invasive/destructive methods of measuring quality of cartilage repair.

Keywords

poly- ϵ -caprolactone, bilayer implant, cartilage repair, electromechanics, Arthro-BST

Introduction

Identifying the right combination of chondrogenic cells and bioactive, biomimetic scaffolds is crucial to achieve a well-integrated and structurally sound repair tissue that resembles native pattern. Furthermore, it is important to successfully regenerate the subchondral bone and its interface.^{1,2} The ideal scaffold construct that creates an appropriate microenvironment while providing mechanical stability for osteochondral lesions has not yet been found. Several aspects including chemical composition, degradation rate, biomechanical strength, and architecture are to be considered.³ Scaffolds can be woven, printed, spun into fibers, or manufactured as gels. Appropriate selection of biomaterials with respect to the targeted tissue is essential. Biomaterials should permit cell recruitment and should provide a 3-dimensional environment that allows for phenotype preservation, differentiation, tissue formation, and maturation and ideally accomplish this while resisting mechanical

forces until the regenerated tissue can take on the load. Thus, it is also necessary to choose a biomaterial with an appropriate degradation rate.⁴ Suitable biomaterials might be subdivided into naturally derived polymers, semisynthetic polymers, and hybrids combining both having specific benefits and disadvantages.⁵ Naturally derived

¹University Medical Center Schleswig-Holstein Campus Lübeck, Clinic for Orthopedics and Trauma Surgery, Lübeck, Germany

²Mayo Clinic, Orthopedic Surgery, Rochester, MN, USA

³Biomedical and Chemical Engineering, Polytechnique Montreal, Montreal, Canada

⁴Biomomentum Inc., Laval, Quebec, Canada

⁵University of Lübeck, Institute of Anatomy, Lübeck, Germany

Corresponding Author:

Jan C. Schagemann, University Medical Center Schleswig Holstein Campus Lübeck, Clinic for Orthopedics and Trauma Surgery, Ratzeburger Allee 160, 23538 Lübeck, Germany.
Email schagemann@cartilage-engineering.de

polymers may preserve cell phenotype and allow for cell adhesion and expression of tissue-specific extracellular matrix (ECM) molecules by expressing appropriate transmembrane receptors.⁶ Therefore, the use of decellularized ECM for the fabrication of scaffolds is attractive also.⁷ Decellularized matrix is biodegradable and does not invoke an immune response while stimulating tissue homeostasis and regeneration. However, maintaining biomechanical properties from these scaffolds when the defects are large and unconfined is a challenge. In contrast, semisynthetic polymers allows for control of biomechanical and biological properties and control of degradation kinetics.

The present work investigates the use of poly- ϵ -caprolactone (PCL). PCL provides initial mechanical stability and has slow degradation kinetics.⁸ PCL maintains this mechanical stability until there is sufficient infiltration and integration of the host tissue.⁹⁻¹¹ It can be machined using rapid prototyping or electrospinning techniques resulting in scaffolds of varying architecture, fiber sizes, and mechanical strength. Prior work has demonstrated biocompatibility with mesenchymal cells and cocultures of chondrogenic and osteogenic cells.¹² Thus, PCL can provide the necessary environments for either bone or cartilage formation and potentially both at the same time.^{13,14} Alterations in pore size, porosity, interconnectivity, fiber diameter, scaffold architecture, stiffness, permeability, and associated biomechanical, biological properties, and biodegradation products including kinetics determine which tissue will be created.^{15,16} It is therefore of great importance to characterize and control macroporous and fibrous textures.¹⁷⁻¹⁹ Nano- or microfibrillar texture can provide specific chemical, biomechanical, and biological signals.²⁰ Seeded or migrating cells respond differently to scaffold geometry and fiber size.⁸ Nanofibrillar structures are similar in dimension to native collagen fibrils. Theoretically, this explains their ability to function as a substitute for the native ECM. PCL nanofibrillar scaffolds seeded with chondrocytes or mesenchymal stem cells (MSCs) support neocartilage formation demonstrating cell anchorage, phenotype preservation, and cartilage-specific gene expression.^{10,21} Li *et al.* found the cytoskeletal organization of chondrocytes cultured in nanofibers to resemble native patterning.⁸ This is important since fibrillar arrangement helps protect cells from stresses caused by compression. Thus, cartilage formation seems to favor a nanotopographical environment.

Coordinated regeneration of cartilage on top of bone alone is the main goal of current research in this area. Creating the boundary layer between the cartilage and bone requires separate consideration.^{19,22} Bilayered or biphasic implants can be tailored to promote the growth necessary to create each individual tissue as well as to form the necessary boundary in between the layers.^{23,24} Despite great advancements in the fabrication of synthetic scaffolds, there remains room for improvement. Therefore, the aim of the

present study was to investigate an anatomically shaped synthetic bilayer scaffold for the regeneration of osteochondral tissue and repair of vast osteochondral defects in a sheep model. We hypothesized that a biomimetic, biodegradable implant comprising a macroporous PCL scaffold mimicking cancellous bone ECM in combination with a nanofibrillar PCL scaffold mimicking cartilage ECM layered on top will create appropriate regenerative conditions for both the chondral and osseous portions of the defect (**Fig. 1**). Our rationale for a synthetic bilayer implant are 3-fold: the individual features of cartilage and bone need to be addressed separately yet in concert to aid in the creation of an appropriate cartilage-bone interface²²; bilayers enable compartmentalized tissue regeneration and repair²⁵⁻²⁸; synthetic scaffolds bear prolonged mechanical stability while serving as temporary conductive templates.^{11,29} To test our hypothesis, the synthetic bilayer was compared to a biologic implant (Chondro-Gide and Orthoss, Geistlich Pharma AG, Wolhusen, Switzerland).

Materials and Methods

Study Design

All experiments were approved by the Ministerium für Landwirtschaft, Umwelt und ländliche Räume (V312-72241.122-15 (109-11/10)). Large artificial osteochondral knee joint defects were created in one knee of each sheep and animals were randomly assigned to the treatment groups ($n = 6$ each) as follows:

Treatment No. 1 (Biologic Control Group). A composite of Chondro-Gide for the regeneration of the cartilage layer combined with Orthoss for the bony lesion functioned as control implant. Treatment No. 1 was generally referred to as a *biologic* implant group.

Treatment No. 2 (Synthetic Experimental Group). A bilayered implant composed of macroporous PCL for the bone portion and a nanofibrillar PCL fleece on top for the cartilage portion of the defect was custom made. Treatment No. 2 was generally referred to as a *synthetic* implant group.

Scaffold Manufacturing

Nanofibrillar PCL. A nanofibrillar (fiber diameter ~400 nm) PCL fleece was fabricated using the classic electrospinning technique. Nanofibrillar scaffolds were composed of a 9.5 wt% homogeneous solution of PCL. This was prepared by dissolving 1.05 g of 80,000 M_n PCL (Sigma Aldrich, St Louis, MO; batch #06725HJ) in 0.8 g *N,N*-dimethylformamide (Fisher Scientific, Waltham, MA), 6.0 g chloroform (Fisher Scientific), and 3.2 g acetone (Fisher Scientific). The solution was allowed to sit for 2 hours and

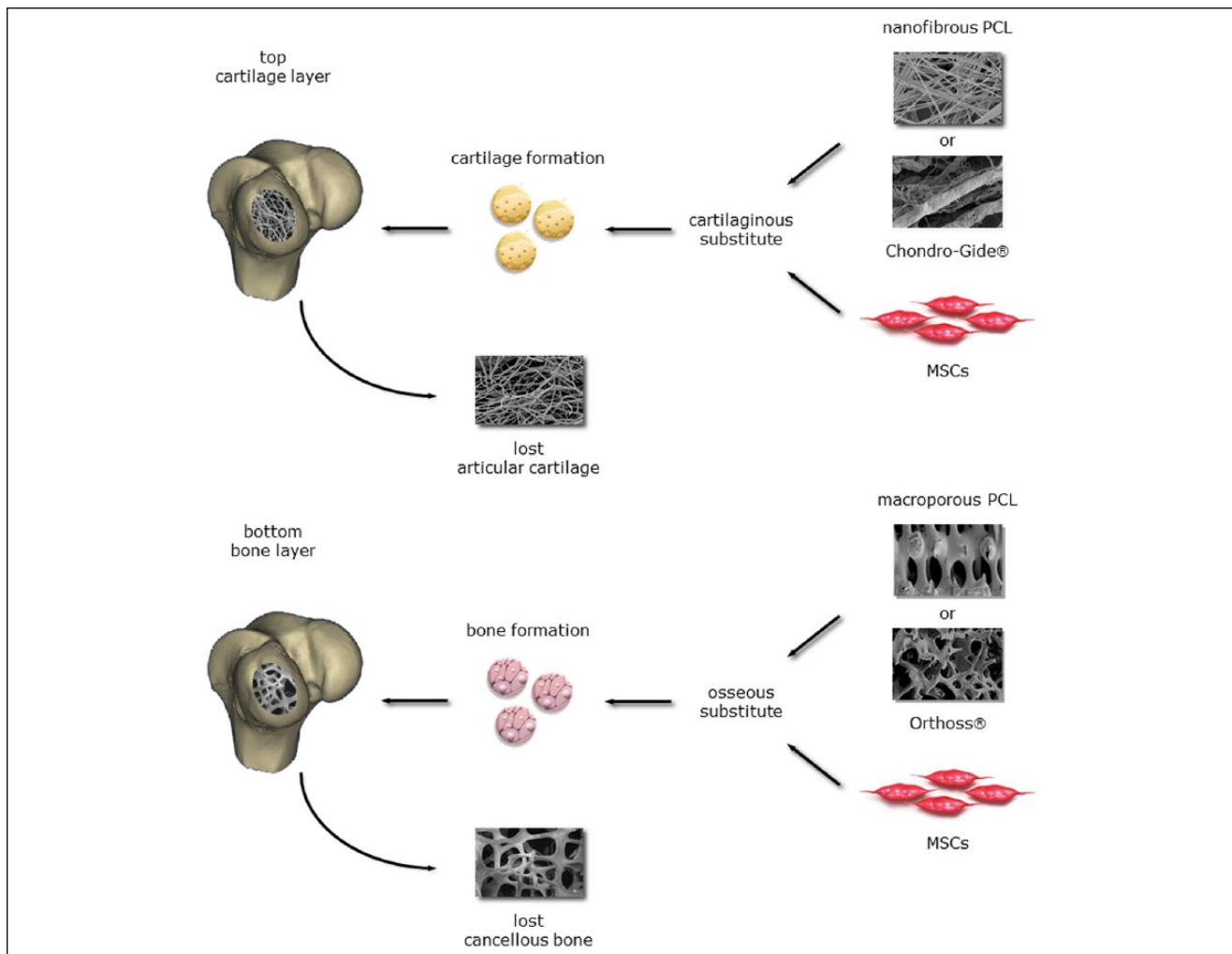


Figure 1. The objective of the present study was to investigate a synthetic bilayer scaffold for the regeneration of osteochondral tissue and repair of large osteochondral defects in a sheep model. We hypothesized that a biomimetic, biodegradable implant comprising of a macroporous PCL scaffold mimicking cancellous bone ECM in combination with a nanofibrous PCL scaffold mimicking cartilage ECM layered on top would create appropriate regenerative conditions for both the chondral and osseous portions of the defect. Combined they might function as an anatomically shaped implant (synthetic implant: Treatment No. 2). The combination of Chondro-Gide and Orthoss functioned as a clinically established control (biologic implant: Treatment No. 1). PCL = poly- ϵ -caprolactone; ECM = extracellular matrix.

then stirred gently for an additional hour. The solution was transferred to a 30 mL glass syringe fitted with a 30-gauge needle. The solution was dispensed at a rate of 3.3 mL/h with a 30 kV electrical field being applied. All fibers were protected by a hood, collected on a glass plate, which was mounted on an aluminum block with the needle tip 15 cm away from the collection plate, and monitored microscopically hourly. The procedure was followed until the sheets reached a thickness of approximately 2 mm.

Macroporous PCL. Using a custom-designed rapid prototyping (RP), molten PCL polymer ($M_w = 65,000$, $M_n = 42,500$; Sigma, St Louis, MO) was extruded by air pressure (630 kPa) through the system's nozzle (\varnothing 200 μ m). A

temperature-controlled reservoir was mounted onto a 3-axis, computer-controlled 3D motion system. Positioning of the system was controlled via a user-defined computer DMC Smart Terminal program (Galil Motion Control, Rocklin, CA) and the motion controller for the servomotors. The system's planar positioning was controlled by x -axis and y -axis servomotors. Material was deposited onto a platform connected to the z -axis servomotor that lowered the platform at the start of each new scaffold layer. Eighty layers resulted in a macroporous PCL matrix of ~ 9 mm thickness, $0^\circ/90^\circ$ architectural geometry with 80% porosity, and ~ 385 μ m pore size.

The final ultrastructure of the different PCL scaffolds was analyzed on a S4700 SEM (Hitachi, Los Angeles, CA)

operating at 3.0 kV. The scaffolds were sterilized with ethylene oxide overnight prior to surgery.

Surgical Procedure

Female sheep ($n = 12$, age: 3-6 years, mean weight: 75.6 kg, range: 62-84 kg) underwent surgery under analgesedation (approximately 0.7 mg/kg ketamine, 0.5 mg/kg xylazine, intramuscularly [IM]) and spinal anesthesia (1.6 mL carbostesin 0.5%). A single injection of 1 g ampicillin and 0.5 g sulbactam was administered intravenously (IV) for infection prophylaxis. The sheep were positioned on their right side with the left limb extended. Left knee joints were opened using a medial parapatellar incision. A standardized cutter was used to create osteochondral defects (width: 6 mm, length: 20 mm, maximum depth: 5 mm) on the weight-bearing area of the medial femoral condyles (L-MFC). Defects were randomly assigned to the 2 different treatment groups.

Treatment No. 1. Granules of Orthoss were soaked in 0.9% NaCl solution until placed in the osseous part of the lesion. Then, a Chondro-Gide sample was cut to size in order to cover the lesion. The matrix was both glued (Tissucol fibrin glue; Baxter/DE) and sutured (PDS 4/0) onto the created defect.

Treatment No. 2. The removed osteochondral fragment was used as an individual template in order to cut the macroporous PCL scaffold to size. A matching nanofibrous fleece of 2 mm thickness was sutured on top using PDS 4/0. The resulting bilayer construct was implanted press-fit into the bleeding defect.

After several cycles of flexion and extension of the knees, the fit of the implants was judged stable and documented as such. At this point, both implants had accumulated a blood clot. The wounds were then closed (vicryl 0 and 2/0, monocryl 3/0) and sheep were housed in small kennels to restrict motion for at least 3 days. There was unrestricted movement thereafter. Metamizole PO was administered for postoperative analgesia. Sheep recovered well from surgery. Nonetheless, seroma ($n = 1$) and wound dehiscence ($n = 1$) was found. The latter needed a revision surgery. In both cases, oral antibiotics were extended until consolidation. Initially, sheep unloaded the operated limb for approximately 4 weeks. Slight limping was observed occasionally. Prolonged analgesia was not necessary. At 2 months, one sheep of the control group developed severe limping of the nonoperated limb. Physical examination revealed a midfoot fracture that was deemed accidental and conservative treatment recommended. Consequently, the affected sheep noticeably loaded mainly the operated limb for at least 3 months afterwards.

After 19½ months postoperation, analgesedation (approximately 0.7 mg/kg ketamine, 0.5 mg/kg xylazine, IM) was



Figure 2. Benchtop version of the Arthro-BST with the testing chamber and the camera-positioning software. The laptop screen shows streaming potential (electrical potential in mV) measured by each of the 37 microelectrodes during indentation and the display of the corresponding Arthro-BST QP (A.U.).

applied as previously described and animals were sacrificed using barbiturate IV (100 mg/kg Trapanal; Byk Gulden, Konstanz, Germany) and potassium (2 mM/kg, 7.45% KCl; Braun, Melsungen, Germany). Two animals had to be euthanized at 13 months (Treatment No. 1) and at 16 months (Treatment No. 2) postoperation due to severe and refractory pneumonia. For these 2 animals only the histologic assessment was performed.

Electromechanics

Sample Preparation. The distal femur was cut through an oblique plane using a vibrating saw to extract the femoral condyles. The condyles were screwed from the bone side onto a cylindrical sample holder ($D = 85$ mm). The sample assembly was then attached into a testing chamber ($D = 19$ cm, $H = 10$ cm) equipped with a camera-registration system (**Fig. 2**; Benchtop Arthro-BST, Biomomentum, Laval, Canada). A position grid was overlaid on the image (Mapping Toolbox software, Biomomentum). A denser sampling of positions was chosen in the vicinity of the repair site than surrounding tissue since previous work has shown that electromechanical properties of articular cartilage vary smoothly over normal surfaces.³⁰ The testing chamber was filled with physiological saline solution (0.15 M, $\text{pH} = 7.4$) and an equilibration time of 15 minutes was allowed prior to the electromechanical mapping. A detailed description of this technique is reported in a recently published article.³¹

Electromechanical Mapping. The Arthro-BST measures compression-induced streaming potentials in articular cartilage using an array of 37 gold microelectrodes lying on a semispherical indenter (effective radius = 3.2 mm, microelectrode density = 5.1 electrodes/mm², microelectrode effective diameter = 75 μm).³¹ The device's quantitative

parameter (QP, A.U.) reflects the amplitude of indentation (number of microelectrodes in contact with cartilage) reached when the sum of the measured electric potential is 100 mV (thus inversely related to the electromechanical function). Therefore, a low QP indicates strong electromechanical properties and a high load-bearing capacity, while a high QP is interpreted as a sign of cartilage degeneration. An abnormally low QP, is interpreted as a sign of abnormally thin cartilage or incomplete cartilage formation. Using the benchtop version of the Arthro-BST (Fig. 2), electromechanical mappings were performed *ex vivo* on all L-MFC and contralateral condyles. With the live-feed of the camera-registration system (spatial registration ± 2 mm), the indenter of the device was manually compressed onto the cartilage surface (for about 1 second, 1 measure per site) at each position and a QP was calculated (Fig. 6).

Diagnostic Mapping. By averaging the QP maps of all 10 contralateral untreated R-MFC (Fig. 6), a reference electromechanical QP map ($QP_R(x,y)$) was calculated for this study (Fig. 7). QP measurements performed at physiologically matched locations over samples from the knees where the defect was created would be considered normal if they fell within the 95% confidence interval (CI) of the reference QP map. The 95% CI should be calculated as $1.96 \times$ standard error (SE). The electromechanical diagnostic parameter (DP) was calculated as the difference between the measured $QP(x,y)$ and the $QP_R(x,y)$ (Fig. 8). With the site-specific reference values subtracted from the QP mapping of the treated femoral condyles, a value close to zero thus corresponds to *normal* cartilage, negative values to *abnormally thin* cartilage (*incomplete repair*), and positive values to *degenerated* cartilage (Fig. 9). Each L-MFC has been divided into 3 distinct regions (center of repair site, internal border of repair site, surrounding cartilage excluding the repair site). The location of the repair site has been established *a posteriori* by superimposing a 6 mm wide rectangular outline. A smaller (1.5 mm offset) rectangular outline (dotted line) is also shown to highlight the center of repair site (Fig. 9).

Histology

Entire joints were examined macroscopically and standardized photographs were taken. While joints were kept moist, former defect sites (L-MFC), the articulating tibial part of the joint (L-MTP), the contralateral (untreated) medial femoral condyle (R-MFC) and medial tibial plateau (R-MTP), and synovial tissue were collected and processed according to the International Cartilage Repair Society (ICRS) recommendations.³² Briefly, samples were fixed in buffered 4% paraformaldehyde protected from light at 5°C, and decalcified in pure ethylenediaminetetraacetic acid (EDTA) at 37°C for 13 weeks. Samples were embedded in paraffin,

and serial coronal sections of 5 μ m thickness were collected from 3 predetermined levels of the repair tissue (anterior, middle, posterior) to take into account obvious repair heterogeneity and site-specific repair response. Sections were stained using hematoxylin-eosin and toluidine blue. Sections were scored by 3 readers in a blinded manner using the ICRS II histological score.

Biochemistry

For biochemical analysis, cartilage biopsies were consistently taken from the most anterior aspect of the former defect site (L-MFC). L-MTP, R-MFC, and R-MTP served as controls. Samples were stored in 1 mL of 50 mM 10 \times phosphate-buffered saline (PBS), 0.1 g sodium acid brought up to 500 mL with H₂O at -4°C until further processing as follows.

sGAG Content. A dimethyl-methylene blue assay (DMMB, Blyscan; Biocolor, Carrickfergus, UK) was used to quantify sGAG content. Samples were rinsed in PBS and then digested with 1 mL of 50 μ g/mL proteinase K (Roche, Indianapolis, IN) in 100 mM K₂HPO₄ (pH 8.0) at 60°C in a water bath for 16 hours. The enzymatic reaction was inactivated at 90°C for 10 minutes. A total of 100 μ L of sample digest was combined with 1 mL DMMB containing dye reagent, mechanically shaken for 30 minutes, and microcentrifuged at 10,000 g for 10 minutes to precipitate sGAG dye complex out of solution. Unbound dye solution was removed and 0.5 mL dissociation reagent was added. Bound dye values were quantified at 656 nm using a SpectraMax Plus spectrophotometer (Molecular Devices, Sunnyvale, CA) and compared against standard curve of chondroitin-4-sulfate (Biocolor). Yield was directly normalized to dsDNA content, dry (dw) and wet weight (ww).

dsDNA Content. The fluorescent picoGreen dsDNA quantification assay (Molecular Probes, Eugene, OR) was used to analyze cell content. Samples were digested according to the sGAG assay. The working reagent solution was prepared as a 200-fold dilution of the concentrated dimethyl sulfoxide solution in 1 \times TE (20 mM Tris-HCl, 2 mM EDTA, pH 7.5). A total of 100 μ L of undiluted sample digest was 1:1 mixed in with working solution and incubated for 5 minutes at room temperature, protected from light, and then excited at 480 nm. Fluorescence emission intensity was measured at 520 nm using a FluoStar Galaxy plate reader (BMG Labtechnologies, Cary, NC) and compared against a standard curve.

Statistical Analysis

Biochemical data were evaluated using ANOVA. Statistical differences between the treatment groups were evaluated

with post hoc testing using least squares means differences Student's *t* test. Histological data were analyzed using 2-factor and 1-factor analysis of variance analysis with and without repeated measures where appropriate. Electromechanical data were analyzed using the electromechanical DP. Statistical differences between the treatment groups were evaluated using a mixed effect model with DP as the response variable, sheep as the random effect, and treatment or regions as the fixed effect. Statistical analyses on electromechanical data were performed with SAS version 9.3 (SAS Institute Inc., Cary, NC). *P* values <0.05 were considered to be significant.

Results

Macroscopic Appearance

In treated joints, variable heterotopic ossifications were found in the soft tissue along the former surgical approach. Synovial hypertrophy, pannus, or signs of graft-versus-host reactions were not observed. Defects were not completely filled. Repair tissue was fibrocartilaginous and heterogeneous in appearance (**Fig. 6**). Both treatments resulted in a partially fragmented surface structure. The implants seemed to be completely remodeled and absent at sacrifice. Joints were void of visible regeneration hypertrophy or bulging, which was independent of implant type. The posterior aspect of L-MFC seemed to repair better than the anterior aspect close to the trochlea. However, in this area occasionally cysts were seen. The untreated joint surfaces in the treated joints as well as the joint surfaces in the contralateral control joints appeared visually normal.

Histology

Microscopic Appearance. Synovial biopsies harvested from the treated joints were void of inflammatory infiltrates (not shown). Toluidine blue histology of the repair tissue depicted a heterogeneous appearance. The former defect sites were almost completely filled. The neocartilage was of fibrous (**Fig. 3F**) and partly of hyaline-like (**Fig. 3D**) morphology, with cells oriented in columns (**Fig. 3B** and **D**). However, the morphology was far from entirely hyaline in nature. The surface structure ranged from irregular (**Fig. 3G**) to smooth (**Fig. 3A**). The lateral and basal integration was primarily good with tidemark formation in both the best (**Fig. 3B**) and worst specimens (**Fig. 3D** and **H**). Also, subchondral bone of trabecular morphology could be observed (**Fig. 3A** and **C**). However, cell clustering at the boundaries (**Fig. 3B, D, and H**), a uniformly flat calcified layer, tidemark duplication, and occasional vascularization (**Fig. 3F**) indicated the beginnings of degeneration. Specimens were void of bold graft hypertrophy or calcification. All these observations were variable and independent of implant design.

Histological Score. Histology revealed a significantly ($P < 0.02$) higher overall ICRS II score for L-MFC of Treatment No. 1 (biologic implant: mean 10.3 ± 0.38 SE) compared to Treatment No. 2 (synthetic implant: mean 8.7 ± 0.45 SE). Repeated-measures ANOVA revealed no significant difference between different predetermined regions of the repair tissue (anterior, middle, posterior) or between the different treatment groups. Moreover, the ICRS II histological scores were significantly different between L-MFC and L-MTP in the context of treated limbs ($P < 0.0006$). For Treatment No. 1, L-MFC had a significantly lower score than R-MFC ($P < 0.01$). Although statistical significance was not found between L-MTP and R-MTP, the score of L-MTP was lower to the point that it was also not significantly different from L-MFC. L-MTP in Treatment No. 1 seemed to perform worse than in Treatment No. 2. Looking at the box plot (**Fig. 4**), this might be due to an outlier in the biologic implant group. For Treatment No. 2, repeated-measures ANOVA revealed a significantly lower score for L-MFC compared to the other biopsy sites ($P < 0.0001$; sheep with missing values were excluded from analysis, as repeated-measures analysis cannot accommodate missing data points). Treatment No. 1 scored higher (**Table 1**) for the parameters: cell morphology (mean 0.86), abnormal calcification/ossification (mean 0.79), and vascularization (mean 0.91), whereas Treatment No. 2 scored higher for matrix staining (mean 0.66), cell morphology (mean 0.62), and vascularization (mean 0.65). The worst parameters for Treatment No. 1 were chondrocyte clustering (mean 0.61), surface architecture (mean 0.62), and formation of tidemark (mean 0.63). The worst parameters for Treatment No. 2 were basal integration (mean 0.47), formation of tidemark (mean 0.34), and mid/deep assessment (mean 0.49).

Biochemistry

L-MFC had significantly less total dsDNA and sGAG normalized to dsDNA compared to controls (L-MTP, R-MFC, R-MTP). This was independent of implant design (**Fig. 5**). Differences between the 2 treatment groups were not significant ($P > 0.05$). When normalizing sGAG to dry and wet weight, there were no significant differences between the individual treatments or biopsy sites. Treatment No. 1 yielded average dsDNA 247 ± 59 SE $\mu\text{g/mL}$, sGAG/weight ww 1.41 ± 0.43 SE/dw 6.47 ± 2.79 SE ng/mg, and Treatment No. 2 yielded average dsDNA 179 ± 59 SE $\mu\text{g/mL}$, sGAG/weight ww 0.46 ± 0.43 SE/dw 1.95 ± 2.79 SE ng/mg. Interestingly, sGAG normalized to dry and wet weight yielded significantly higher in R-MTP compared to L-MFC in the synthetic implant group.

Electromechanics

Contralateral Surfaces and DP Threshold. For both treatments, QP values measured at the repair sites (L-MFC)

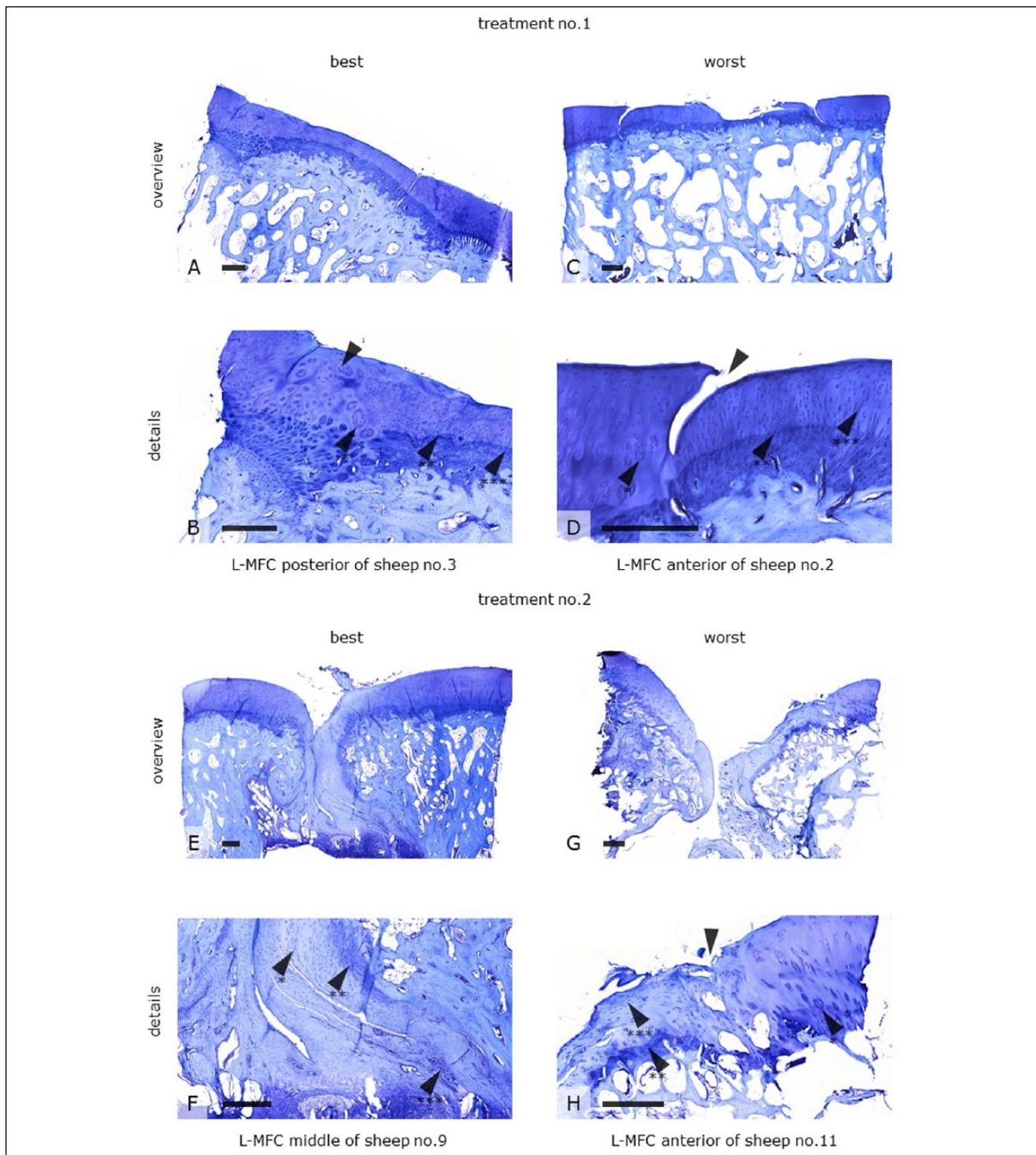


Figure 3. Toluidine blue histology of tissue repair found in former defect sites (L-MFC) after being treated either with a biologic (Treatment No. 1) or a synthetic (Treatment No. 2) bilayer implant 19 months postoperatively. The figure shows examples of best versus worst specimens for both treatment groups. The defect sites were almost completely restored with a fibrous (**F** arrow*, **H** arrow**) and partly hyaline-like neocartilage with cells oriented in columns (**B** and **D** arrows**). The surface was either irregular (**G**) or smooth (**A**). The lateral integration was primarily good (**B** arrow). Lateral dehiscence was also found (**D** arrow). Tidemark formation (arrows**) indicated a sound cartilage-bone interface even in the worst specimens (**H** arrow**). Cell clusters at the boundaries respectively within the adjacent cartilage (**B**, **D**, **H** arrow*), a uniformly flat calcified layer, tidemark duplication, and occasional vascularization (**F** arrow**) indicated degenerative processes. These observations were variable and independent of implant design. Scale bars: 500 µm. L-MFC = left medial femoral condyle.

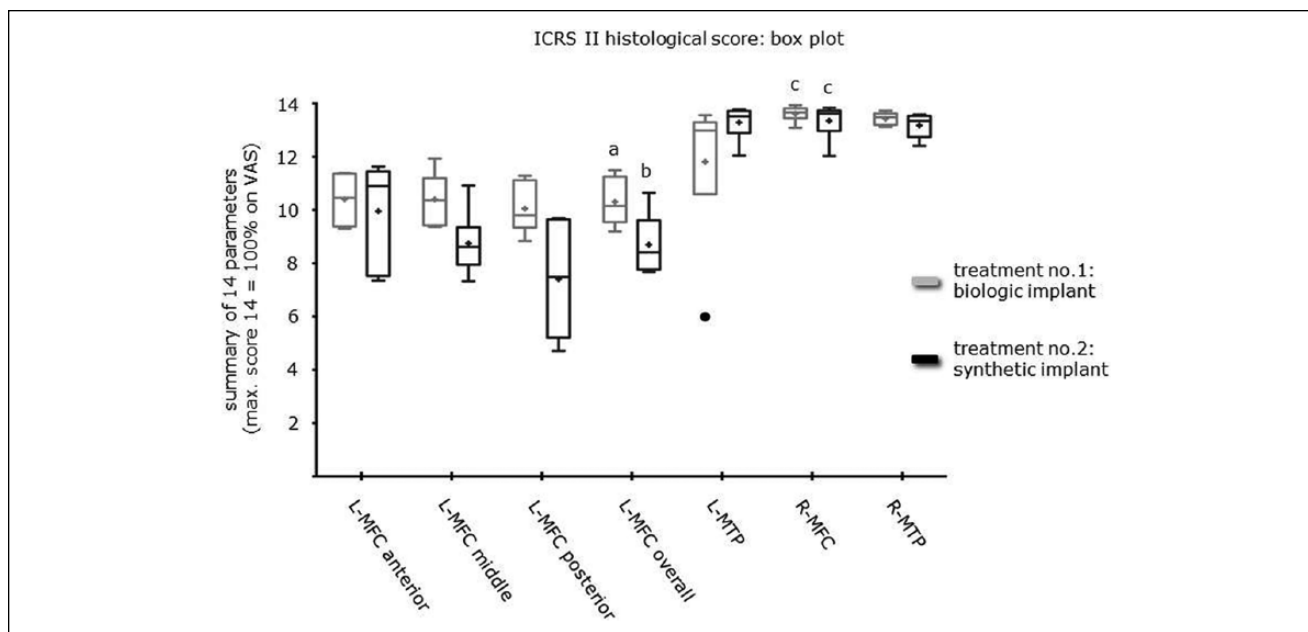


Figure 4. Box plot using the Tukey method representing the ICRS II histological scoring of the different biopsy sites. L-MFC of the biologic implant group had a significantly higher yield compared to L-MFC of the synthetic implant group (a/b: $P < 0.02$). No statistical significance was found between different predetermined levels of the repair tissue (anterior, middle, posterior) or between the different treatment groups. For both treatment groups, L-MFC had a significantly lower yield than R-MFC (a/c: $P < 0.01$; b/c: $P < 0.0001$). ICRS = International Cartilage Repair Society score; L-MFC = left medial femoral condyle; R-MFC = right medial femoral condyle.

Table I. Single Parameters of the ICRS II Histological Score (Maximum Score 1 = 100%) for Treatment No. 1 (Biologic Implant) and Treatment No. 2 (Synthetic Implant).

| Histological Parameter | ICRS II Histological Score: Parameters | |
|---|--|-----------------|
| | Mean Score for L-MFC | |
| | Treatment No. 1 | Treatment No. 2 |
| 1. Tissue morphology | 0.73 | 0.58 |
| 2. Matrix staining | 0.71 | 0.66 |
| 3. Cell morphology | 0.86 | 0.62 |
| 4. Chondrocyte clustering | 0.61 | 0.58 |
| 5. Surface architecture | 0.62 | 0.59 |
| 6. Basal integration | 0.72 | 0.47 |
| 7. Formation of a tidemark | 0.63 | 0.34 |
| 8. Subchondral bone abnormalities | 0.70 | 0.60 |
| 9. Inflammation | 0.98 | 0.85 |
| 10. Abnormal calcification/ossification | 0.79 | 0.57 |
| 11. Vascularization | 0.91 | 0.65 |
| 12. Surface/superficial assessment | 0.68 | 0.59 |
| 13. Mid/deep assessment | 0.69 | 0.49 |
| 14. Overall assessment | 0.69 | 0.53 |

ICRS = International Cartilage Repair Society score; L-MFC = left medial femoral condyle.

were lower than those obtained for the contralateral surface (R-MFC; **Fig. 6**). **Figure 7** shows the reference Electromechanical QP map ($QP_R(x,y)$) obtained by averaging QPs measured on the right (untreated) medial femoral condyles ($n = 10$). Also, SE were calculated at each position of the map ($n < 10$) considering the homogeneity of the SE of the entire articular surface, and the overall variation on the QPs measured were given by averaging all of the SE. With regard to the averaged SE, a 95% CI ($1.96 \times SE$) was obtained as the threshold at which the DP could detect either degeneration or incomplete repair. Indeed, in our study—10 contralateral surfaces (R-MFC)—the DP threshold calculated is 1.37. Therefore, a DP between -1.37 and 1.37 indicates *normal* cartilage with a 95% CI. A DP > 1.37 indicates *degenerated* cartilage, and DP < -1.37 indicates *incomplete repair respectively thin* cartilage with a 95% CI.

Treatments. For Treatment No. 1, overall DP of the repair site was -1.50 ± 2.9 SD ($n = 266$) indicating slightly better regeneration than Treatment No. 2, with an overall DP of the repair site of -2.62 ± 2.7 SD ($n = 255$; **Fig. 8**). DP of the center of the repair site was -2.26 ± 2.8 SD ($n = 114$) for Treatment No. 1 and -3.87 ± 2.6 SD ($n = 111$) for Treatment No. 2 (**Fig. 9**), while the DP of the internal border of repair site was -0.91 ± 2.8 SD ($n = 152$) for Treatment No. 1 and -1.60 ± 2.3 SD ($n = 144$) for Treatment No. 2. These results were not significantly different (overall: $P = 0.068$, center:

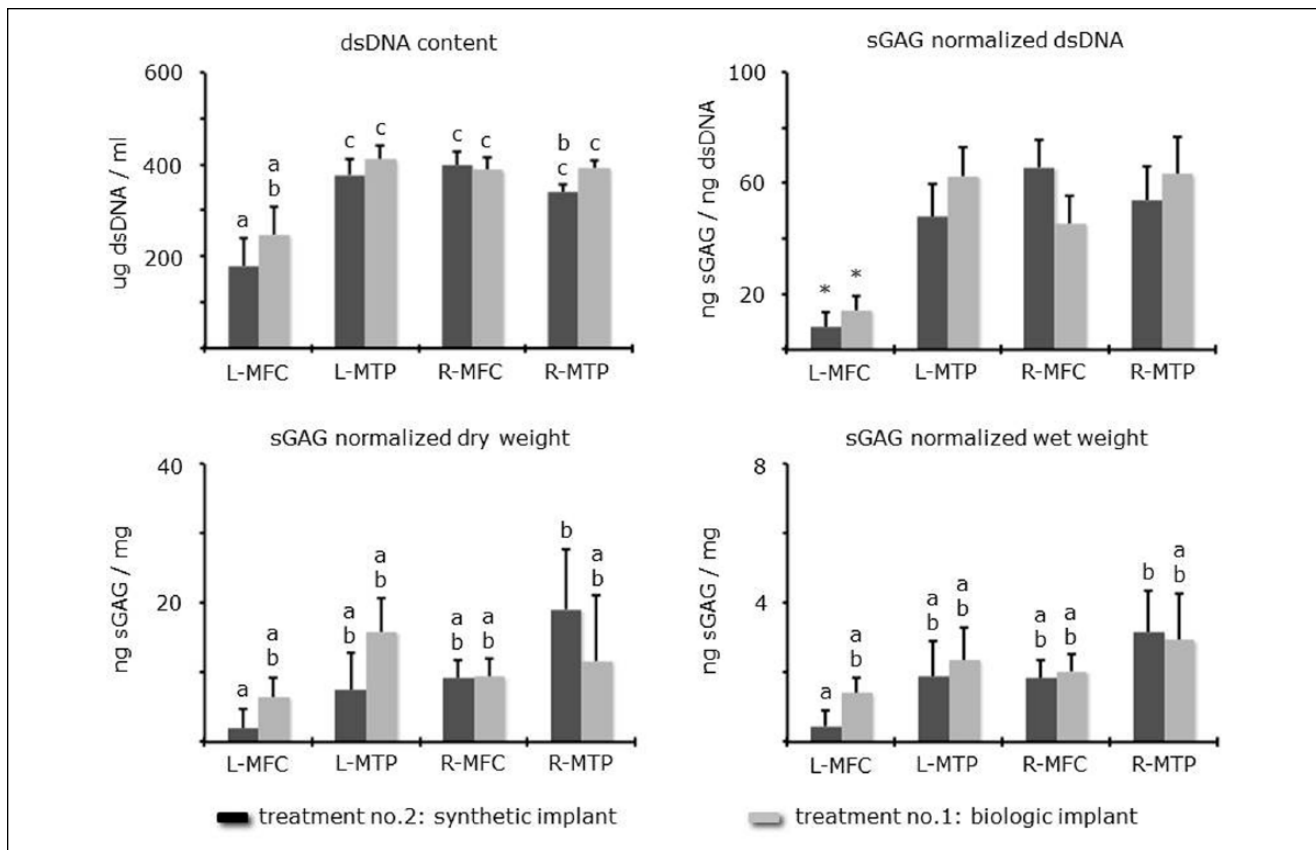


Figure 5. dsDNA and sGAG per site versus treatment presented as means \pm SE. Differences are either by letter (a, b, c) or asterisk ($P < 0.05$). If there is no letter in common, then they were significantly different.

$P = 0.084$; internal border: $P = 0.15$) between both treatments. However, there was a significant difference between the electromechanical DP of the center and the internal border of repair (Treatment No. 1: $P = 0.0001$; Treatment No. 2: $P < 0.0001$). For both treatment groups, Arthro-BST revealed early signs of degeneration of the surrounding cartilage bordering the repair site on the L-MFC (**Fig. 8**), where DP was 1.55 ± 2.92 SD ($n = 922$) for Treatment No. 1 and 2.08 ± 3.15 SD ($n = 963$) for Treatment No. 2 (**Fig. 9**). The treatment type did not result in significant differences in degradation of the surrounding cartilage ($P = 0.47$).

Discussion

For both treatments, electromechanical QP values, total dsDNA and sGAG normalized to dsDNA, and histological scores measured at the repair sites were statistically lower than those obtained from the untreated sites. The electromechanical QP decreases with thickness. When the cartilage layer is thin, only a limited area of the spherical indenter enters in contact with the cartilage surface during indentation while the streaming potential generated becomes very high (due to the high compression in terms of strain of the

thin cartilage under the point of contact). This results in abnormally low QP, that is, negative DP. Therefore, low QPs and negative DPs occur where thickness is less than normal. We propose that neocartilage showing a DP between 1.37 and -1.37 should have been interpreted as normal: In order to determine if neocartilage resembles native cartilage, a diagnostic parameter was calculated. The diagnostic parameter consisted of subtracting the measured value by a reference value. In theory, if neocartilage would resemble native cartilage, the diagnostic parameter shall be zero, which would be considered as normal. However, our reference value consists of using 10 controls (untreated medial femoral condyles); therefore, we needed to calculate the natural variability of our reference (normal) DP range around 0. To calculate the natural variability between these 10 samples, we calculated the SE at each matched position. This allowed us to obtain the overall variability on the QPs measured in the 10 controls. With regard to a 95% CI ($1.96 \times$ SE), which is the most used confidence interval in orthopedic field,³³ we obtained the upper and lower limits of our DP normal range, which is -1.37 to 1.37 . It is important to note the radial integration of the repair, which can be done by comparing the Arthro-BST DP of the center to that of the internal border of

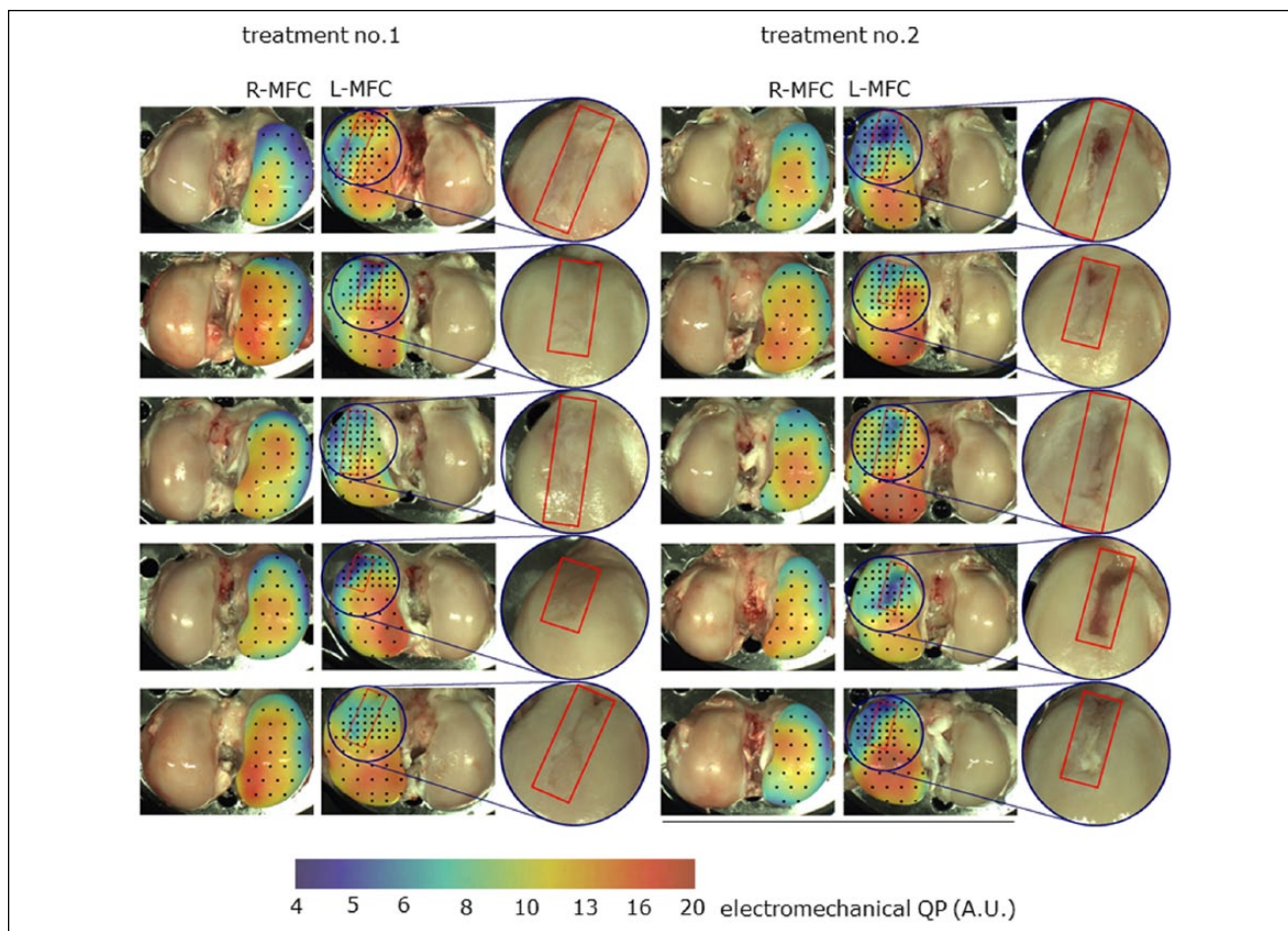


Figure 6. Electromechanical QP mapping of R-MFC (untreated) and L-MFC (treated) of each sheep for both treatments. A logarithmic scale from 4 (blue, detection threshold) to 20 (red, max value in this study) was used. Sixty percent transparency was applied to the mapping layer so that articular surface landmarks remain visible through mapping. The associated scale was also blended with 60% transparency with the average cartilage surface color, which allows for a better matching of the scale colors to those of the mapping. The black dots represent all test positions performed. The repair site has been outlined in red on the treated L-MFC and has been zoomed in by 200%. L-MFC = left medial femoral condyle; R-MFC = right medial femoral condyle.

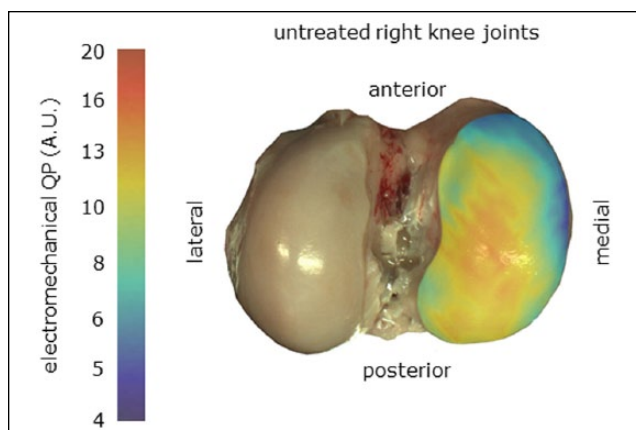


Figure 7. Reference electromechanical QP map, $QP_R(x,y)$, created by interpolating and averaging cartographic measurements from the 10 untreated R-MFC (presented in Fig. 6). R-MFC = right medial femoral condyle.

the repair site. A significant difference between those 2 regions in favor of the border site reflects better regeneration at the site and thus integration. Also, there was considerable degeneration occurring at the posterior side of the L-MFC. Since the defect was on this side, we believe that the animal was compensating and thus overloading the posterior side. Comparing the treatment groups, the biologic implant had a significantly higher histological score and a numerically higher DP, closer to normal, demonstrating better regeneration than the synthetic implant. There were no significant biochemical differences between the 2 treatment groups. When normalizing sGAG to weight, values were close to contralateral controls indicating good regenerative capacity within the defect sites and the ability of the implants to degrade appropriately. This supports our observations of islands of fine osteochondral regeneration. However, this finding could either be the result of incomplete regeneration or the onset of degeneration. Incomplete regeneration is

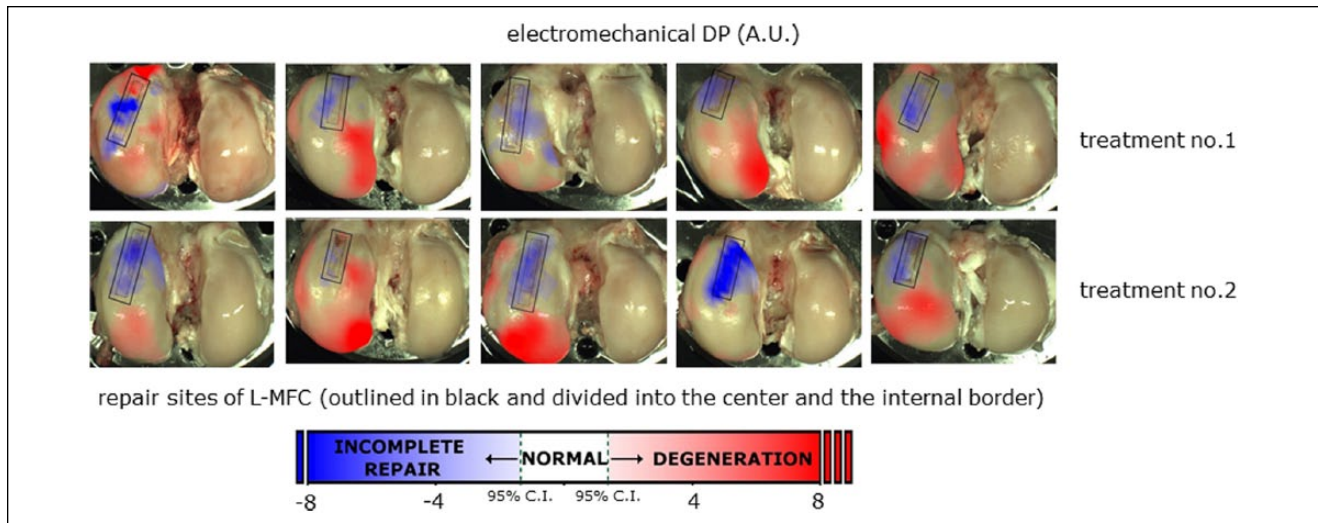


Figure 8. Electromechanical DP mapping of joints for Treatment No. 1 and Treatment No. 2. Arthro-BST DP was calculated as the difference between the measured QP and the reference Arthro-BST QP, $QP_R(x,y)$, that is, the average of all untreated contralateral joints (R-MFC) as presented in **Figure 7**. The repair site has been outlined in black and divided into 2 regions delimited by a dotted line. The inner region of the dotted line is the center of repair and the outer region of the dotted line is the internal border of repair. R-MFC = right medial femoral condyle.

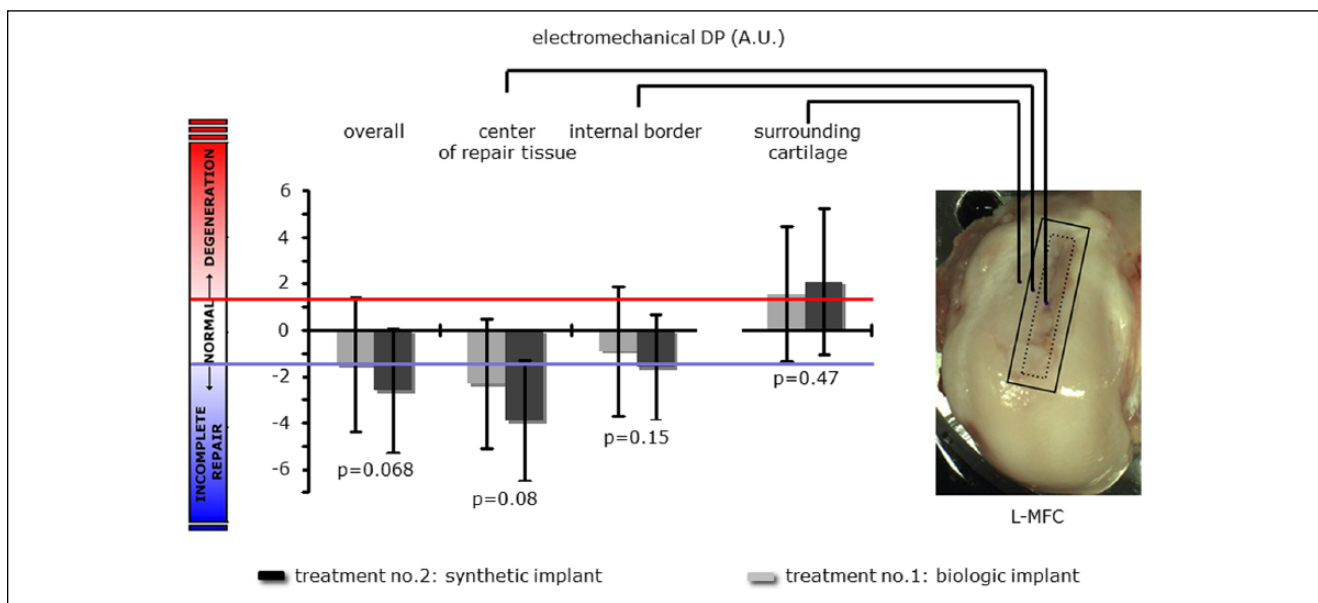


Figure 9. Electromechanical DP (average \pm SD) for the L-MFC subdivided into the center of repair site, the internal border of repair site, and the surrounding cartilage. The threshold for distinguishing normal from incomplete repair or degeneration was set at 1.37 corresponding to 95% CI formulation ($1.96 \times SE$). Using this threshold degenerated cartilage has DP > 1.37 , normal cartilage has DP between -1.37 and 1.37 , and abnormally thin (incomplete repair) cartilage has DP < 1.37 . L-MFC = left medial femoral condyle; CI = confidence interval.

unlikely since our follow-up was over 19 months. Degeneration is more likely. This is supported by our Arthro-BST results, which revealed early signs of degeneration of the cartilage bordering the repair sites. It is also supported by our histological findings, which revealed signs typical of

osteoarthritis. However, degenerative changes were also found in contralateral controls. Therefore, we cannot conclude whether the regeneration was poor leading to degradation or that the regenerated tissue was affected by degenerative changes that were already occurring in the

joint. Future studies should include biopsies at intermediate time points for information about changes due to aging. However, both implants failed to promote a true hyaline cartilage layer, tidemark, and trabecular subchondral bone. Aspects of success and failure of a construct are multifactorial, as follows.

Lesion Size and Animal Model

As summarized by Reinholz *et al.*, the key issue in the selection of an appropriate animal model is to match the model to the question being investigated and the hypothesis to be tested.²² It is general consensus that large animal models such as sheep are most appropriate in preclinical cartilage repair studies, while no animal model permits direct application to humans. However, it is crucial to establish critical size defects as they do not heal spontaneously.^{25,34,35} Our own observations are partly inconsistent: our previous hydrogel study on mature sheep demonstrated that untreated critical size osteochondral defects (diameter: 6 mm, depth: 12 mm) were not restored properly,³⁶ whereas even larger untreated osteochondral defects (diameter: 8 mm, depth: 13 mm) in another study also on mature sheep showed a healing response (submitted). In order to avoid lesion size as a factor of uncertainty, a decision was made for vast osteochondral defects (width: 6 mm, length: 20 mm, maximum depth: 5 mm). The length allowed for cross-section histological analysis of more anterior and posterior parts of the treated femoral condyle as recommended by the ICRS.³²

Biomaterials

Literature supports the repair of cartilage and bone with various PCL scaffolds.²⁴ PCL is highly supportive to MSCs in terms of cell anchorage, phenotype preservation, cartilage, and bone-specific gene expression.^{10,12-15,21} PCL has excellent biomechanical properties and slow degradation kinetics. This led to our hypotheses that a combination of macroporous and nanofibrous PCL would be a suitable bilayer implant. This hypothesis was supported by our previous findings that even unrefined nanofibrous PCL promoted the expression of cartilage-specific ECM by bone marrow-derived MSCs *in vitro*.³⁷ In the case of an osseous lesion, even acellular PCL constructs can regenerate bone.^{34,38} Shao *et al.* combined porous PCL with tricalcium phosphate seeded with bone marrow-derived MSCs using fibrin glue to treat osteochondral defects in a rabbit model.²⁵ The bone formation at 6 months postoperative was excellent. However, neocartilage surface regularity and structural integrity was poor. Other studies demonstrated cell-seeded PCL scaffolds to have a greater chondrogenic capacity than unseeded scaffolds.³⁹ Unrefined nanofibrous PCL is incapable of recruiting cells *in vitro*.³⁷ In conclusion, the random nanofibrous structure of our cartilage PCL

layer, although meant to be biomimetic and despite its chondrogenic potential, could impede cellular infiltration.⁴⁰ Thus, the initial acellularity of our implants could be one drawback. However, this is most likely not the entire rationale as both treatment groups demonstrated cell infiltration with cell morphology being one of the best histological parameters in common.

Cartilage-Bone Interface

Successful osteochondral tissue regeneration requires respecting the cartilage-bone and host-graft interfaces.⁴¹⁻⁴⁴ Techniques that produce fibrocartilage also promote little tidemark and calcified cartilage regeneration creating a less stable cartilage-bone interface.¹ Our histological results support the importance of the interaction at this tissue interface as there was poor tidemark formation. And the histological results indicated fibrocartilaginous tissue. However, both our implants showed excellent lateral integration. This might be due to the bilayer design that matches the surrounding tissue to reduce discontinuities at the interface.⁴⁵

Zonal Organization

Bioprinting and patterning in 3 dimensions of various layers can construct specific tissue architectures.⁴⁶ Bilayered implants allow for tissue-specific layers of the construct to be tailored to promote individual growth of 2 distinct tissue types on a single integrated construct.^{23,24,47} Layers can each be multiphasic by addition of bioactive macromolecules such as growth factors and/or (decellularized) ECM on different parts of the scaffold.^{6,7} Besides conventional fabrication techniques,⁴⁸ including rapid prototyping^{9,49,50} and solution electrospinning,^{17,20,51,52} methods such as melt electrospinning or electrospraying could have allowed greater control in optimizing fiber orientation, matrix porosity, and biomechanical and biochemical properties in our implants.^{52,53} It is uncontested that nanofibers can provide chemical, biomechanical, and biological signals and that they can act as functional and conductive substitutes.^{8,10,20,21} However, in contrast to our randomly oriented PCL nanofibers, aligned fibers could better promote oriented neocartilage that would provide mechanical and cellular properties with greater similarity to superficial or deep zone cartilage where collagen fibers are aligned.⁵⁴ Thus, we could incorporate highly organized microscale structures *bottom-up*^{8,55} similar to natural conditions and to create distinct zones in our synthetic implants.^{56,57} Our bilayer implant that is biomimetic anatomically speaking is a considerable first step. However, the variations in proteoglycan and collagen networks, and the distinctly organized cells that have zone-specific metabolic activity, are the most defining characteristics for determining zonal variation of hyaline cartilage.¹⁹ Altogether this suggests that it would be best to

design a scaffold with a similar zonal architecture and to use different cells for different zones. Although we applied a PCL implant with a biomimetic yet uniform cartilage layer, we could see cellular infiltration and zonal organization typical for hyaline cartilage. *In vitro*, zonal tissue organization is tangible using combination of hydrogels and hybrids in layering or gradient models.⁵⁸⁻⁶² However, if placed *in vivo*, any construct would be subject to complex environmental processes and signals that are uncontrollable.¹⁹ Additionally, *in vivo* remodeling also involves the scaffolds' ultrastructure, and stratified constructs that were successful *in vitro* may not be able to maintain their zonal organization or disintegrated *in vivo*.^{45,63}

Cell Source

Pooling and amplification of primary chondrocytes is detrimental to cell phenotype. Chondrocytes from different zones are incapable of expressing zone-specific ECM.^{64,65} This supports the use of MSCs because they retain the ability to create zone-specific ECM.⁶⁶ Since our acellular implants accommodated MSCs they theoretically should be able to form some zonal organization even throughout the uniform scaffold.⁴¹ As summarized by Hollander *et al.*,⁴⁴ bone marrow-derived MSCs have a tendency to differentiate into hypertrophic chondrocytes in the deep zones of articular cartilage, whereas the same population of MSCs located in the upper layers remain in a prehypertrophic state. Moreover, the superficial zone seems to originate from MSCs that have a different phenotype than MSCs found in the deeper zones.⁶⁷ However, exogenous signals appear to be insufficient in order to establish a true zonal organization starting from bone marrow.¹⁹ Dynamic seeding protocols⁶⁸ and physical and chemical gradients within the scaffolds may help overcome inhomogeneous cell seeding and/or recruitment, thereby improving zone-specific cellular organization.⁶⁹

In conclusion, the anatomically shaped design of the synthetic implant was meant to promote compartmented tissue regeneration. As a major limitation, few lesions were treated. Therefore, our study is of pilot nature. Nonetheless, both implants allowed for cell infiltration. The regeneration of bone and cartilage was simultaneously induced. However, the structural integrity of the neo-tissue still requires improvement. Except for histological scoring, no significant differences were observed in the quality of the regenerated tissue among treatment groups. Our results indicated better regeneration for the biologic versus synthetic implants. The implementation of additional zonal properties within the bilayer constructs could advance true zonal formation and osteochondral tissue engineering. As a secondary aspect, our study suggests suitability of Arthro-BST for the assessment of cartilage repair techniques in an animal model. The findings were supported by traditional

outcome measures as recommended by the ICRS. However, a specifically designed study is needed to validate the reliability of Arthro-BST for the analysis of cartilage repair tissue.

Acknowledgments and Funding

All experiments were approved by the Ministerium für Landwirtschaft, Umwelt und ländliche Räume (V312-72241.122-15(109-11/10)). Funding was provided by the University of Lübeck (E43-2008) and a MSD Sharp & Dohme scholarship. Chondro-Gide and Orthoss were kindly provided by Geistlich Pharma AG. There was however no conflict of interest between the two parties. We thank T. Asmus for excellent histological work, S. Schlottau for surgical assistance, and J. S. Fitzsimmons for statistical advises. We are obliged to C. Erggelet, T. Gemoll, J. Gille, C. Hoemann, A. Larouche, E. Mrosek, S. Paul, G. Reinholz, S. Roberts, M. Russlies, D. Theisen-Kunde, and A. R. Thoreson (in alphabetical order) for technical, intellectual, and unconditioned support.

Declaration of Conflicting Interests

The author(s) declared the following potential conflicts of interest with respect to the research, authorship, and/or publication of this article: E. Quenneville and M. Garon are coowners of Biomomentum Inc.

Ethical Approval

Ethical approval for this study was waived by Ministerium für Landwirtschaft, Umwelt und ländliche Räume (V312-72241.122-15 (109-11/10)).

Animal Welfare

The present study followed international, national, and/or institutional guidelines for humane animal treatment and complied with relevant legislation.

References

1. Hoemann CD, Lafantaisie-Favreau CH, Lascau-Coman V, Chen G, Guzman-Morales J. The cartilage-bone interface. *J Knee Surg.* 2012;25:85-97.
2. Gomoll AH, Madry H, Knutsen G, van Dijk N, Seil R, Brittberg M, *et al.* The subchondral bone in articular cartilage repair: current problems in the surgical management. *Knee Surg Sports Traumatol Arthrosc.* 2010;18:434-47.
3. Seo SJ, Mahapatra C, Singh RK, Knowles JC, Kim HW. Strategies for osteochondral repair: focus on scaffolds. *J Tissue Eng.* 2014;5:2041731414541850.
4. Sittinger M, Hutmacher DW, Risbud MV. Current strategies for cell delivery in cartilage and bone regeneration. *Curr Opin Biotechnol.* 2004;15:411-8.
5. Tuan RS, Chen AF, Klatt BA. Cartilage regeneration. *J Am Acad Orthop Surg.* 2013;21:303-11.
6. Schagemann JC, Kurz H, Casper ME, Stone JS, Dadsetan M, Yu-Long S, *et al.* The effect of scaffold composition on the early structural characteristics of chondrocytes and expression of adhesion molecules. *Biomaterials.* 2010;31:2798-805.

7. Benders KE, van Weeren PR, Badylak SF, Saris DB, Dhert WJ, Malda J. Extracellular matrix scaffolds for cartilage and bone regeneration. *Trends Biotechnol.* 2013;31:169-76.
8. Li WJ, Jiang YJ, Tuan RS. Chondrocyte phenotype in engineered fibrous matrix is regulated by fiber size. *Tissue Eng.* 2006;12:1775-85.
9. Huttmacher DW, Schantz T, Zein I, Ng KW, Teoh SH, Tan KC. Mechanical properties and cell cultural response of polycaprolactone scaffolds designed and fabricated via fused deposition modeling. *J Biomed Mater Res.* 2001;55:203-16.
10. Li WJ, Danielson KG, Alexander PG, Tuan RS. Biological response of chondrocytes cultured in three-dimensional nanofibrous poly(epsilon-caprolactone) scaffolds. *J Biomed Mater Res A.* 2003;67:1105-14.
11. Huttmacher DW. Scaffolds in tissue engineering bone and cartilage. *Biomaterials.* 2000;21:2529-43.
12. Cao T, Ho KH, Teoh SH. Scaffold design and in vitro study of osteochondral coculture in a three-dimensional porous polycaprolactone scaffold fabricated by fused deposition modeling. *Tissue Eng.* 2003;9(Suppl 1):S103-12.
13. Hsu SH, Yen HJ, Tseng CS, Cheng CS, Tsai CL. Evaluation of the growth of chondrocytes and osteoblasts seeded into precision scaffolds fabricated by fused deposition manufacturing. *J Biomed Mater Res B Appl Biomater.* 2007;80:519-27.
14. Endres M, Huttmacher DW, Salgado AJ, Kaps C, Ringe J, Reis RL, et al. Osteogenic induction of human bone marrow-derived mesenchymal progenitor cells in novel synthetic polymer-hydrogel matrices. *Tissue Eng.* 2003;9:689-702.
15. Mitsak AG, Kempainen JM, Harris MT, Hollister SJ. Effect of polycaprolactone scaffold permeability on bone regeneration in vivo. *Tissue Eng Part A.* 2011;17:1831-9.
16. Goldstein AS, Zhu G, Morris GE, Meszlenyi RK, Mikos AG. Effect of osteoblastic culture conditions on the structure of poly(DL-lactic-co-glycolic acid) foam scaffolds. *Tissue Eng.* 1999;5:421-34.
17. Kumbar SG, James R, Nukavarapu SP, Laurencin CT. Electrospun nanofiber scaffolds: engineering soft tissues. *Biomed Mater.* 2008;3:034002.
18. Lu T, Li Y, Chen T. Techniques for fabrication and construction of three-dimensional scaffolds for tissue engineering. *Int J Nanomedicine.* 2013;8:337-50.
19. Klein TJ, Malda J, Sah RL, Huttmacher DW. Tissue engineering of articular cartilage with biomimetic zones. *Tissue Eng Part B Rev.* 2009;15:143-57.
20. Prabhakaran MP, Ghasemi-Mobarakeh L, Ramakrishna S. Electrospun composite nanofibers for tissue regeneration. *J Nanosci Nanotechnol.* 2011;11:3039-57.
21. Li WJ, Tuli R, Okafor C, Derfoul A, Danielson KG, Hall DJ, et al. A three-dimensional nanofibrous scaffold for cartilage tissue engineering using human mesenchymal stem cells. *Biomaterials.* 2005;26:599-609.
22. Reinholz GG, Lu L, Saris DB, Yaszemski MJ, O'Driscoll SW. Animal models for cartilage reconstruction. *Biomaterials.* 2004;25:1511-21.
23. O'Shea TM, Miao X. Bilayered scaffolds for osteochondral tissue engineering. *Tissue Eng Part B Rev.* 2008;14:447-64.
24. Swieszkowski W, Tuan BH, Kurzydowski KJ, Huttmacher DW. Repair and regeneration of osteochondral defects in the articular joints. *Biomol Eng.* 2007;24:489-95.
25. Shao X, Goh JC, Huttmacher DW, Lee EH, Zigang G. Repair of large articular osteochondral defects using hybrid scaffolds and bone marrow-derived mesenchymal stem cells in a rabbit model. *Tissue Eng.* 2006;12:1539-51.
26. Kandel RA, Grynepas M, Pilliar R, Lee J, Wang J, Waldman S, et al. Repair of osteochondral defects with biphasic cartilage-calcium polyphosphate constructs in a sheep model. *Biomaterials.* 2006;27:4120-31.
27. Mardones RM, Reinholz GG, Fitzsimmons JS, Zobitz ME, An KN, Lewallen DG, et al. Development of a biologic prosthetic composite for cartilage repair. *Tissue Eng.* 2005;11:1368-78.
28. Frenkel SR, Bradica G, Brekke JH, Goldman SM, Ieska K, Issack P, et al. Regeneration of articular cartilage—evaluation of osteochondral defect repair in the rabbit using multiphasic implants. *Osteoarthritis Cartilage.* 2005;13:798-807.
29. Lu L, Zhu X, Valenzuela RG, Currier BL, Yaszemski MJ. Biodegradable polymer scaffolds for cartilage tissue engineering. *Clin Orthop Relat Res.* 2001;(391 Suppl):S251-70.
30. Sim S, Picard G, Quenneville E, Garon M, Buschmann MD. The spatial pattern of articular cartilage electromechanical properties in the stifle joint is similar in three different species. *Transactions of the 59th Annual Meeting of the Orthopaedic Research Society, San Antonio, TX; 2013.*
31. Sim S, Chevrier A, Garon M, Quenneville E, Yaroshinsky A, Hoemann CD, et al. Non-destructive electromechanical assessment (Arthro-BST) of human articular cartilage correlates with histological scores and biomechanical properties. *Osteoarthritis Cartilage.* 2014;22:1926-35.
32. Hoemann CD, Kandel R, Roberts S, Saris DB, Creemers LB, Mainil-Varlet P, et al. International Cartilage Repair Society (ICRS) recommended guidelines for histological endpoints for cartilage repair studies in animal models and clinical trials. *Cartilage.* 2011;2:153-72.
33. Vavken P, Heinrich KM, Koppelhuber C, Rois S, Dorotka R. The use of confidence intervals in reporting orthopaedic research findings. *Clin Orthop Relat Res.* 2009;467:3334-9.
34. Mrosek EH, Schagemann JC, Chung HW, Fitzsimmons JS, Yaszemski MJ, Mardones RM, et al. Porous tantalum and poly-epsilon-caprolactone biocomposites for osteochondral defect repair: preliminary studies in rabbits. *J Orthop Res.* 2010;28:141-8.
35. Shao XX, Huttmacher DW, Ho ST, Goh JC, Lee EH. Evaluation of a hybrid scaffold/cell construct in repair of high-load-bearing osteochondral defects in rabbits. *Biomaterials.* 2006;27:1071-80.
36. Schagemann JC, Erggelet C, Chung HW, Lahm A, Kurz H, Mrosek EH. Cell-laden and cell-free biopolymer hydrogel for the treatment of osteochondral defects in a sheep model. *Tissue Eng Part A.* 2009;15:75-82.
37. Schagemann JC, Paul S, Casper ME, Kaps C, Rohwedel J, Fehr M, et al. Chondrogenic differentiation of bone marrow derived MSCs via biomimetic and bioactive poly-epsilon-caprolactone scaffolds. *Biomaterials.* 2013;101:1620-8.
38. Feczko P, Hangody L, Varga J, Bartha L, Dioszegi Z, Bodo G, et al. Experimental results of donor site filling for autologous osteochondral mosaicplasty. *Arthroscopy.* 2003;19:755-61.
39. Li WJ, Chiang H, Kuo TF, Lee HS, Jiang CC, Tuan RS. Evaluation of articular cartilage repair using biodegradable nanofibrous scaffolds in a swine model: a pilot study. *J Tissue Eng Regen Med.* 2009;3:1-10.

40. Garrigues NW, Little D, Sanchez-Adams J, Ruch DS, Guilak F. Electrospun cartilage-derived matrix scaffolds for cartilage tissue engineering. *J Biomed Mater Res A*. 2014;102:3998-4008.
41. Mikos AG, Herring SW, Ochareon P, Elisseeff J, Lu HH, Kandel R, *et al*. Engineering complex tissues. *Tissue Eng*. 2006;12:3307-39.
42. Grayson WL, Chao PH, Marolt D, Kaplan DL, Vunjak-Novakovic G. Engineering custom-designed osteochondral tissue grafts. *Trends Biotechnol*. 2008;26:181-9.
43. Nukavarapu SP, Dorcemus DL. Osteochondral tissue engineering: current strategies and challenges. *Biotechnol Adv*. 2013;31:706-21.
44. Hollander AP, Dickinson SC, Kafienah W. Stem cells and cartilage development: complexities of a simple tissue. *Stem Cells*. 2010;28:1992-6.
45. Obradovic B, Martin I, Padera RF, Treppo S, Freed LE, Vunjak-Novakovic G. Integration of engineered cartilage. *J Orthop Res*. 2001;19:1089-97.
46. Derby B. Printing and prototyping of tissues and scaffolds. *Science*. 2012;338:921-6.
47. Keeney M, Pandit A. The osteochondral junction and its repair via bi-phasic tissue engineering scaffolds. *Tissue Eng Part B Rev*. 2009;15:55-73.
48. Karande TS, Ong JL, Agrawal CM. Diffusion in musculoskeletal tissue engineering scaffolds: design issues related to porosity, permeability, architecture, and nutrient mixing. *Ann Biomed Eng*. 2004;32:1728-43.
49. Zein I, Huttmacher DW, Tan KC, Teoh SH. Fused deposition modeling of novel scaffold architectures for tissue engineering applications. *Biomaterials*. 2002;23:1169-85.
50. Huttmacher DW. Scaffold design and fabrication technologies for engineering tissues—state of the art and future perspectives. *J Biomater Sci Polym Ed*. 2001;12:107-24.
51. Murugan R, Ramakrishna S. Nano-featured scaffolds for tissue engineering: a review of spinning methodologies. *Tissue Eng*. 2006;12:435-47.
52. Brown TD, Dalton PD, Huttmacher DW. Direct writing by way of melt electrospinning. *Adv Mater*. 2011;23:5651-7.
53. Huttmacher DW, Dalton PD. Melt electrospinning. *Chem Asian J*. 2011;6:44-56.
54. Wise JK, Yarin AL, Megaridis CM, Cho M. Chondrogenic differentiation of human mesenchymal stem cells on oriented nanofibrous scaffolds: engineering the superficial zone of articular cartilage. *Tissue Eng Part A*. 2009;15:913-21.
55. Nichol JW, Khademhosseini A. Modular tissue engineering: engineering biological tissues from the bottom up. *Soft Matter*. 2009;5:1312-9.
56. Barthes J, Ozcelik H, Hindie M, Ndreu-Halili A, Hasan A, Vrana NE. Cell microenvironment engineering and monitoring for tissue engineering and regenerative medicine: the recent advances. *Biomed Res Int*. 2014;921905.
57. Zorlutuna P, Annabi N, Camci-Unal G, Nikkhah M, Cha JM, Nichol JW, *et al*. Microfabricated biomaterials for engineering 3D tissues. *Adv Mater*. 2012;24:1782-804.
58. Sharma B, Elisseeff JH. Engineering structurally organized cartilage and bone tissues. *Ann Biomed Eng*. 2004;32:148-59.
59. Kim TK, Sharma B, Williams CG, Ruffner MA, Malik A, McFarland EG, *et al*. Experimental model for cartilage tissue engineering to regenerate the zonal organization of articular cartilage. *Osteoarthritis Cartilage*. 2003;11:653-64.
60. Ng KW, Wang CC, Mauck RL, Kelly TA, Chahine NO, Costa KD, *et al*. A layered agarose approach to fabricate depth-dependent inhomogeneity in chondrocyte-seeded constructs. *J Orthop Res*. 2005;23:134-41.
61. Mironov V, Reis N, Derby B. Review: bioprinting: a beginning. *Tissue Eng*. 2006;12:631-4.
62. Cohen DL, Malone E, Lipson H, Bonassar LJ. Direct free-form fabrication of seeded hydrogels in arbitrary geometries. *Tissue Eng*. 2006;12:1325-35.
63. Chawla K, Klein TJ, Schumacher BL, Jadin KD, Shah BH, Nakagawa K, *et al*. Short-term retention of labeled chondrocyte subpopulations in stratified tissue-engineered cartilaginous constructs implanted in vivo in mini-pigs. *Tissue Eng*. 2007;13:1525-37.
64. Hayes AJ, Hall A, Brown L, Tubo R, Caterson B. Macromolecular organization and in vitro growth characteristics of scaffold-free neocartilage grafts. *J Histochem Cytochem*. 2007;55:853-66.
65. Blewis ME, Schumacher BL, Klein TJ, Schmidt TA, Voegtline MS, Sah RL. Microenvironment regulation of PRG4 phenotype of chondrocytes. *J Orthop Res*. 2007;25:685-95.
66. Pittenger MF, Mackay AM, Beck SC, Jaiswal RK, Douglas R, Mosca JD, *et al*. Multilineage potential of adult human mesenchymal stem cells. *Science*. 1999;284:143-7.
67. Lee SY, Nakagawa T, Reddi AH. Mesenchymal progenitor cells derived from synovium and infrapatellar fat pad as a source for superficial zone cartilage tissue engineering: analysis of superficial zone protein/lubricin expression. *Tissue Eng Part A*. 2010;16:317-25.
68. Vunjak-Novakovic G, Obradovic B, Martin I, Bursac PM, Langer R, Freed LE. Dynamic cell seeding of polymer scaffolds for cartilage tissue engineering. *Biotechnol Prog*. 1998;14:193-202.
69. Singh M, Berkland C, Detamore MS. Strategies and applications for incorporating physical and chemical signal gradients in tissue engineering. *Tissue Eng Part B Rev*. 2008;14:341-66.